Modern Physics Letters B
Vol. 27, No. 27 (2013) 1350199 (8 pages)

DOI: 10.1142/S0217984913501996

THE STRUCTURE, MAGNETISM AND CONDUCTIVITY OF $Li_3V_2(PO_4)_3$: A THEORETICAL AND EXPERIMENTAL STUDY

ZHI-PING LIN*,‡, YU-JUN ZHAO† and YAN-MING ZHAO†

*School of Physics and Optoelectronic Engineering,
Guangdong University of Technology, Guangzhou 510090, China
†Department of Physics, South China University of Technology,
Guangzhou 510640, China
‡zhipinglphy@gdut.edu.cn

Received 12 June 2013
Revised 16 August 2013
Accepted 16 August 2013
Published 14 October 2013

In this paper, we present a combination of first-principles and experimental investigations on the structural, magnetic and electronic properties of monoclinic $Li_3V_2(PO_4)_3$. The change of dielectric constant indicates that the structural phase transition appear around the temperature 120°C. The first-principles calculation and magnetic measurement display that $Li_3V_2(PO_4)_3$ is a compound with weak ferromagnetism, with Curie constant of $C = 0.004$ and Curie temperature of 140 K. The experimental and theoretical results demonstrated that the $Li_3V_2(PO_4)_3$ is a typical semiconductor.

Keywords: First-principles; lithium vanadium phosphate; magnetism; conductivity.

PACS Number(s): 71.15.Mb

Transition metal phosphates have generated considerable interest as cathodes for rechargeable lithium batteries. In recent years, vanadium phosphate-based cathodes had been extensively studied.[1–4] These materials are regarded to be safer than typical commercial cathode materials. $Li_3V_2(PO_4)_3$ in various phases have been investigated as cathodes for lithium batteries.[5–8] Monoclinic $Li_3V_2(PO_4)_3$ displays the highest capacity, and its full reversible extraction has been achieved at fast rates.[9,10] Saïdi *et al.*[9] have investigated the properties of the monoclinic lithium vanadium phosphate using X-ray diffraction and electrochemical method and observed a potential > 4.6 when the last lithium has been extracted. Yin *et al.*[11] investigated the correlation and the structural features in the series of single-phase materials $Li_{3-y}V_2(PO_4)_3$ with the electrochemical voltage-composition profile and mainly highlighted the importance of ion–ion interactions in determining phase transitions. The experimental investigations indicate that the carbon-coating can

enhance the electrode reaction reversibility as well as the capacity retention and rate performance.[12,13] However, the study on the magnetic properties and electrical conductivity of the monoclinic $Li_3V_2(PO_4)_3$ is insufficient. As we know that computational simulations have the advantage in compensating the real experiments that one can fully control over the relevant variables. What is especially worth mentioning is the first-principle calculation that has obtained the huge breakthrough in understanding the lithium-ion batteries' materials and other materials.[14–16] Shi *et al.*[15] present the investigation of the structural, magnetic and electronic properties of $LiFePO_4$ olivine. Bacq *et al.*[17,18] studied the impact of electronic correlations on the structural stability, magnetism and voltage of $LiCoPO_4$ battery. In this paper, the magnetic properties and conductivity of $Li_3V_2(PO_4)_3$ have been investigated from experiment and calculation. The magnetic ground state and electronic structure were obtained by using the first-principle calculation approach and experimental method.

The calculations are based on density-functional theory with the general gradient approximation (GGA + U) using Perdew–Wang form for the exchange correlation energy[19,20] as implemented in the Vienna *ab initio* simulation package (VASP).[19–23] The GGA + U approach can treat correlation effects in localized d electrons of V ions by a Hubbard-like term to account for the quasi-atomic character of the localized orbital. Therefore, this method makes more applicable to transition metal compound to correct the energies and to improve the band gap. In the calculation, a series of U value change from 2 eV to 5 eV. It is found that the value of the energy gap strongly depends on the U value. The calculating results show that the band gap is better when the U value is set as 3.5 eV. Hence, we employed $U = 3.5$ eV to obtain the magnetic structure and electronic structure of ground state. The interactions between valence electrons and ions were represented with the projector augmented wave (PAW) pseudo-potentials. The structure was fully relaxed with respect to internal and external cell parameters. The wave functions were expanded in plane waves with an energy cut-off 420 eV. Brillouin zone integration was performed with a $2 \times 2 \times 1$ Monkhorst–Pack mesh. The relaxation of lattice is stopped until the forces of each ion are converged to 5 meV $Å^{-1}$. The magnetic measurement is performed by a quantum SQUID magnetometer at a field of 300 Oe. The electronic conductivity measurement was adopted with a RTS-8 linear four-point probe measurement system. The specimens used for electronic conductivity measurement were disk-shaped pellet with 10 mm in diameter and 1.5 mm in thickness. The electrical conductivity of $Li_3V_2(PO_4)_3$ powders is nearly 10^{-4} S/cm. The dielectric and resistance measurement was studied by an HP 4294A impedance analyzer with a small ac signal of 1 V, and the specimen is treated by coating with silver glue in the surface of disk-shaped pellet to make electrodes.

The $Li_3V_2(PO_4)_3$ has the monoclinic structure with the space group $P21/n$. In this structure, each unit cell contains four chemical formula units of $Li_3V_2(PO_4)_3$, all the Li, V, P, O atoms occupy Wyckoff position 4e with different coordinates. This monoclinic structure comprises a framework of metal octahedra and phosphate

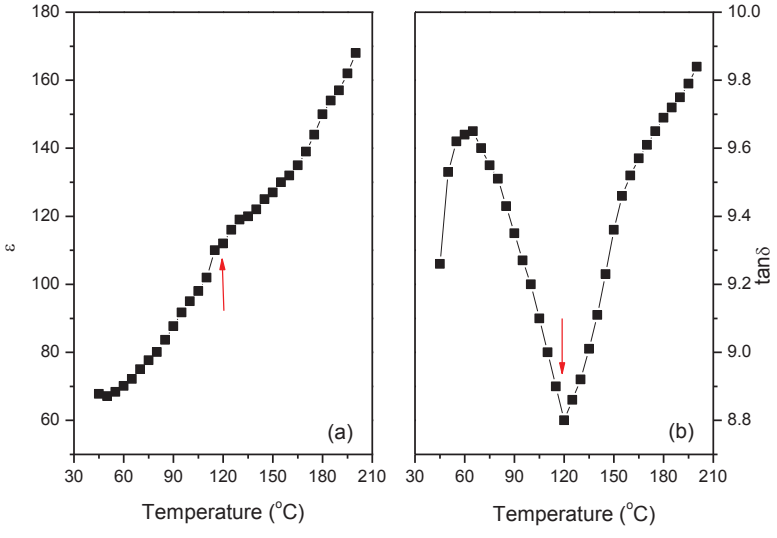

Fig. 1. (Color online) The relationship of dielectric constant and temperature for $Li_3V_2(PO_4)_3$ under 100 KHz: (a) resistive component; (b) loss component.

Table 1. Lattice parameters of $Li_3V_2(PO_4)_3$ and $V_2(PO_4)_3$. Atomic coordinates is given in units.

	$Li_3V_2(PO_4)_3$ (Calc.)	$Li_3V_2(PO_4)_3$ (Expt.[11])	$V_2(PO_4)_3$ (Calc.)
a (Å)	8.7837	8.6079	8.6154
b (Å)	8.6420	8.5957	8.7942
c (Å)	12.1048	12.040	11.410
	$\beta = 90.585$	$\beta = 90.586$	$\alpha = 89.302$, $\beta = 90.627$, $\gamma = 89.401$
V (Å^3)	905.32	890.85	863.17 (Expt.[11] 829.6)

tetrahedra sharing oxygen vertices. Each VO_6 octahedron is surrounded by six PO_4 tetrahedronwhereas each PO_4 tetrahedron is surrounded with four VO_6 octahedron. This configuration forms a three-dimensional network. Electric charge carriers, lithium ions, are located in the cavities within the framework. The dielectric constant and temperature relation can reflect the structural phase transition and the microstructural change of compound. Hence, we investigated the dielectric constant and temperature relation of $Li_3V_2(PO_4)_3$ under 100 KHz frequency, as shown in Fig. 1. It can be seen that the dielectric constant has a transition around 120°C, indicating a structural phase transition at this temperature. It implies that the structure of cathode is stable under room temperature. The optimized crystal parameters for $Li_3V_2(PO_4)_3$ and $V_2(PO_4)_3$ are listed in Table 1, together with the experimental values of $Li_3V_2(PO_4)_3$.[11] The computed crystal parameters for $Li_3V_2(PO_4)_3$ are also basically in agreement with the experimental values. But the structure of de-lithium phase has a distorted triclinic phase, with $\alpha = 89.302°$,

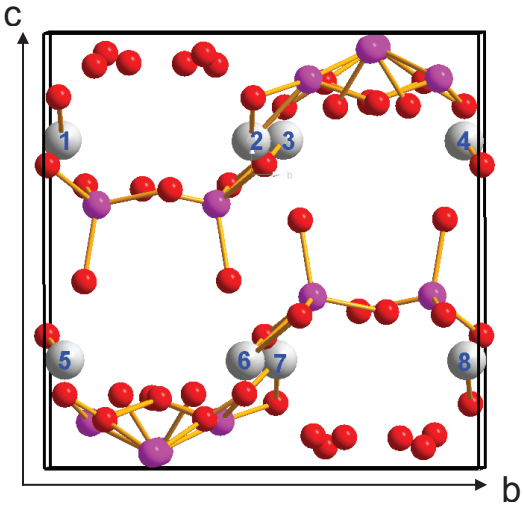

Fig. 2. (Color online) Schematic drawing of the eight vanadium atoms in the cell of $Li_3V_2(PO_4)_3$.

$\beta = 90.627°$, $\gamma = 89.401°$, respectively. The calculated volume of the unit cell is 1.6% larger than that of the experimental values for $Li_3V_2(PO_4)_3$. In fact, it should be noted that the calculated volume change during delithium is rather small (6.14%), in line with the experimental value (6.87%, see Ref. 9). This small volume change implies that $Li_3V_2(PO_4)_3$ could achieve a long lifetime for lithium ion battery when used as the cathode material.

The ground-state spin configuration of $Li_3V_2(PO_4)_3$ is investigated by first-principles calculation and magnetic susceptibility measurement. We calculate all possible collinear magnetic configurations consisting and including the spin–orbit coupling using a chemical cell and lattice parameters fixed at the relaxed values but allowing the magnetic moments of its eight V atoms to relax, and the eight V atoms are shown in Fig. 2. The V-atoms in $Li_3V_2(PO_4)_3$ also form a 2D square lattice in the b–c plane with the nearest neighbor V–V distance 4.313 Å. The interlayer V–V distance along a-axis is 6.573 Å and it is larger than that of the distance between layers. The calculated energies of three stable spin configurations are listed in Table 2, and the total energies of other spin configurations are either nonconverged or even higher than the one without spin polarization. From our results, it can be seen clearly that the total energies of spin configurations are about 90 meV $\sim$ 200 meV lower than that of nonspin configuration. The energy of S-P1 spin configuration is lowest, with a rather small local magnetic moment ($\mu_{\text{eff}} \approx 0.333\ \mu_B$/atom). Hence, the S-P1 spin configuration that is the typical weak ferromagnetic structure should be the spin ground state configuration, which is in agreement with the structure characteristic.

The magnetic susceptibility of $Li_3V_2(PO_4)_3$ exhibit a typical Curie–Weiss behavior for $T > 140$ K. The magnetic susceptibility χ can then be expressed as a

Table 2. The possible spin polarization configurations and the difference of energy between spin configurations and non-spin configuration.

	1	2	3	4	5	6	7	8	ΔE (eV)	μ_{eff} (μ_{B}/atom)
S-P1	↑	↑	↑	↑	↑	↑	↑	↑	−0.213	0.333
S-P2	↑	↑	↑	↑	↓	↓	↓	↓	−0.100	0.028
S-P3	↑	↓	↑	↓	↑	↓	↑	↓	−0.090	0.148

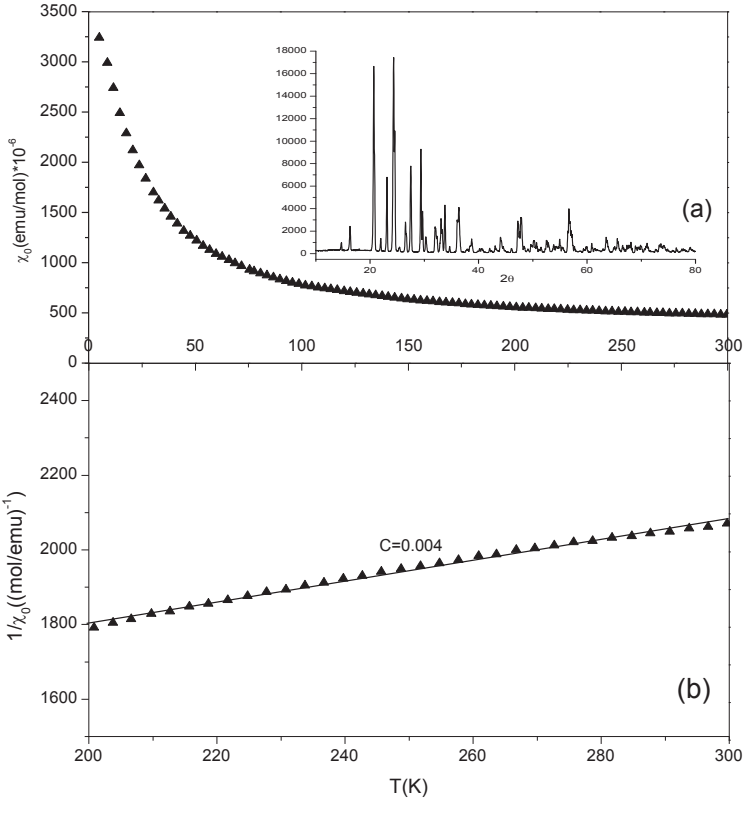

Fig. 3. (a) The thermal evolution of the molar magnetic susceptibility for the $Li_3V_2(PO_4)_3$ phase is shown; (b) the relationship of the reciprocal of the magnetic susceptibility with the temperatures. The subplot is the XRD date.

function of $1/T$:

$$\chi = \frac{C}{T} + N\alpha\,,$$

where C is the Curie constant and $N\alpha$ is the correction that is applied to take into account the temperature independent paramagnetism at high temperatures. The $N\alpha$ value was obtained by extrapolating χ to $1/T = 0$ in the plot of χ as a function of $1/T$. The reciprocal of the temperature independent paramagnetism versus corrected magnetic susceptibility is plotted against T in Fig. 3. The linear

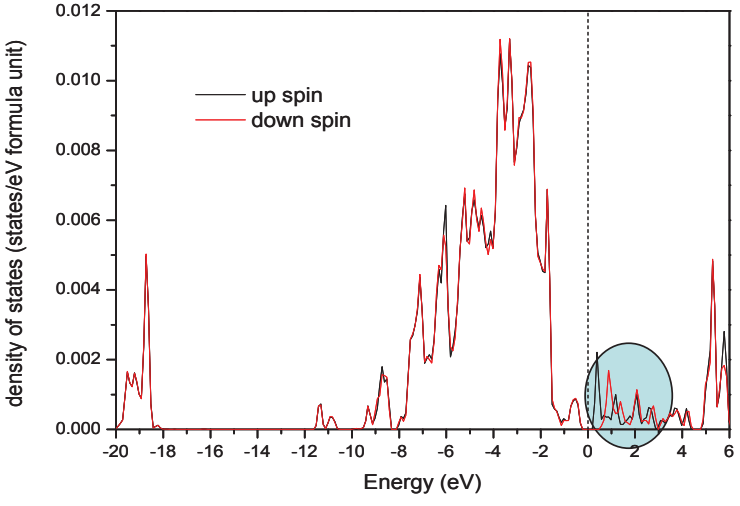

Fig. 4. Density of states for the $Li_3V_2(PO_4)_3$. The Fermi level is set to zero.

fit of the data points above $T = 140$ K leads to a Curie constant $C = 0.004$. As shown in Fig. 4, the plot of the molar magnetic susceptibility data as a function of temperature suggests that $Li_3V_2(PO_4)_3$ is a compound with weak ferromagnetism. Spin density of states (shown in Fig. 4) also display that the spin polarization of V atoms change the distribution of state near the bottom of the conduction band, which this spin-polarized state gives rise to weak-ferromagnetism.

The density of state is shown in Fig. 4. The Fermi level lies in the band gap with 0.59 eV, which is formed by hybridization of vanadium *d*-states, phosphorus *p*-states and oxygen *p*-states. Therefore, the compound shows the semiconductor characteristic. The resistance of most materials changes with temperature. And then the resistance and temperature (frequency) measurement was also studied by an HP 4294A impedance analyzer with a small ac signal of 1 V. The experimental specimen is a disk-shaped pellet of 1.5 mm in thickness and 10 mm in diameter and is treated by coating with silver paster in the surface of disk-shaped pellet to make electrodes. The resistance and temperature (frequency) relation is shown in Figs. 5(a) and 5(b). The resistance decreases exponentially with the increasing temperature, where $R = R_0 e^{-\alpha T}$. It illustrates that $Li_3V_2(PO_4)_3$ is a typical semiconductor. The number of charge carrier will increase with temperature build-up. Hence, the increase of operating temperature is advantageous for improving the electrochemical characteristic of cathode material.

In this paper, we have investigated the structural, magnetic and electronic properties of monoclinic $Li_3V_2(PO_4)_3$ by first-principles calculation and experiment. Results show that the dielectric constant has the structural phase transition around the temperature 120°C. The first-principles calculation and magnetic measurement display that $Li_3V_2(PO_4)_3$ is a compound with weak ferromagnetism, where the

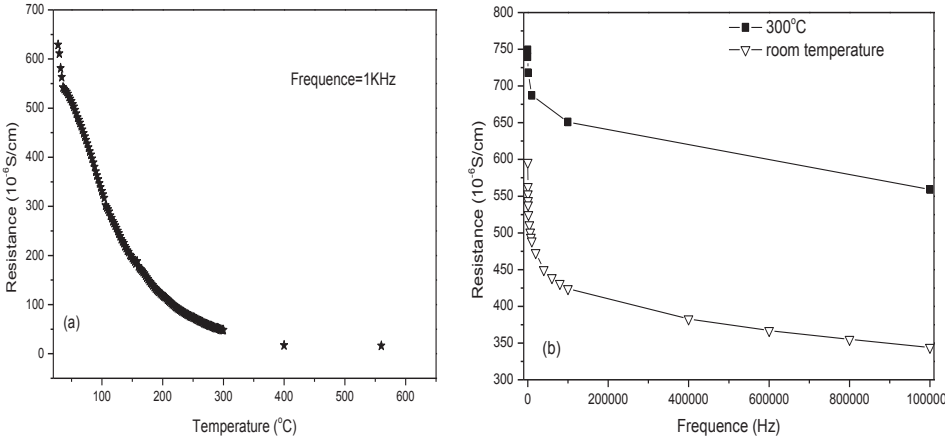

(a) (b)

Fig. 5. (a) Resistance and temperature characteristic of $Li_3V_2(PO_4)_3$ under 1 KHz; (b) resistance and frequency characteristic of $Li_3V_2(PO_4)_3$ under room temperature.

Curie constant is $C = 0.004$ and the Curie temperature is 140 K. The experimental and theoretical result also display that the $Li_3V_2(PO_4)_3$ is a typical semiconductor with negative temperature coefficient. The width of band gap is 0.59 eV. With increasing temperature the resistance decreases exponentially.

Acknowledgments

This work was funded by NSFC Grant (Nos. 11204042, 51172077 and 11174082) through NSFC Committee of China and the Foundation (No. S2011020000521) through the Science and Technology Bureau of Guangdong Government, respectively.

References

1. A. K. Padhi *et al.*, *J. Electrochem. Soc.* **144** (1997) 1188.
2. A. K. Ivanov-Shits and J. Schoonman, *Solid State Ionics* **91** (1996) 93.
3. A. Yamada and K. Hinokuma, *J. Electrochem. Soc.* **148** (2001) A224.
4. H. Huang, S.-C. Yin and L. F. Nazar, *Electrochem. Solid-State Lett.* **4** (2001) A170.
5. M. Y. Saïdi *et al.*, *J. Power Source* **119** (2003) 266.
6. D. Morgan and G. Ceder *et al.*, *Chem. Mater.* **14** (2002) 4684.
7. D. Morgan and G. Ceder *et al.*, *J. Power Source* **119** (2003) 755.
8. J. Barker, M. Y. Saïdi and J. L. Swaoyer, *J. Electrochem. Soc.* **150** (2003) A1394.
9. M. Y. Saïdi *et al.*, *Electrochem. Solid-State Lett.* **5** (2002) A149.
10. H. Huang, S.-C. Yin, Y. Kerr and L. F. Nazar, *Adv. Mater.* **14** (2002) 1525.
11. S.-C. Yin *et al.*, *J. Am. Chem. Soc.* **125** (2003) 10402.
12. P. Fu *et al.*, *Electrochemica Acta* **52** (2007) 5281.
13. P. Fu *et al.*, *J. Power Sources* **162** (2006) 651.
14. S. Shi *et al.*, *Phys. Rev. B* **67** (2003) 115130.

15. S. Shi *et al.*, *Phys. Rev. B* **71** (2005) 144404.
16. J. Santamaria, J. Garcia-Barriocanal, Z. Sefrioui and C. Leon, *Int. J. Mod. Phys. B* **27** (2013) 1330013.
17. O. L. Bacq, A. Pasturel and O. Bengone, *Phys. Rev. B* **69** (2004) 245107.
18. P. Deniard *et al.*, *J. Phys. Chem. Solids* **65** (2004) 229.
19. J. P. Perdew *et al.*, *Phys. Rev. B* **46** (1992) 6671.
20. G. Kresse and J. Hafner, *Phys. Rev. B* **47** (1993) 558.
21. G. Kresse and J. Hafner, *Phys. Rev. B* **49** (1994) 14251.
22. G. Kresse and J. Furthmuller, *Comput. Mater. Sci.* **6** (1996) 15.
23. G. Kresse and J. Furthmuller, *Phys. Rev. B* **54** (1996) 11169.